Malaysian Journal of Chemistry, 2025, Vol. 27(5), 95-109
(Special Issue: *5th IKMPB Online Symposium, IKMPB 2025*)

Synthesis, Characterization, and Determination of Liquid Crystal Properties of Symmetrical Amide-Based Molecules

Tan Zhe Cong[1], Zuhair Jamain[1]* and Melati Khairuddean[2]
[1]Organic Synthesis and Advanced Materials (OSAM) Research Group, Faculty of Science and Technology, Universiti Malaysia Sabah (UMS), 88400 Kota Kinabalu, Sabah, Malaysia
[2]School of Chemical Sciences, Universiti Sains Malaysia (USM), 11800 Penang, Malaysia
*Corresponding author (e-mail: zuhairjamain@ums.edu.my)

A series of new hybrid amide-based liquid crystals was successfully synthesized and characterized. The 4-alkoxybenzoic acids (**1a–b**) were synthesized via the alkylation and subsequent saponification of methyl 4-hydroxybenzoate using heptyl and decyl bromide, respectively. The amidation of compounds **1a–b** with thionyl chloride and 1,4-phenylenediamine yielded N,N'-(1,4-phenylene)bis(4-substituted benzamides) (**2a–b**), which possess a symmetrical structure. These compounds were characterized using Fourier transform infrared (FTIR) spectroscopy, nuclear magnetic resonance (NMR) spectroscopy, and CHN elemental analysis. The determination and conformation of liquid crystal properties were achieved using polarized optical microscope (POM) and differential scanning calorimetry (DSC). The main functional groups in compounds **2a–b** can be seen in the FT-IR spectrum by the characteristic stretching vibrations of C*sp3*-H, C=O, C=C, and C-O stretching at ~ 2900 and 2850, 1700, 1600, and 1290 cm^{-1}, respectively. In the ^{1}H-NMR spectrum, a singlet peak at δ 9.24 ppm showed the presence of amino groups in the compound, indicating the successful formation of amide linkage. Compounds **2a–b** show nematic phase with schlieren texture at 131.4 and 130.9 °C, respectively. The DSC thermograms of compounds **2a–b** demonstrate two transitions, thus confirming the presence liquid crystals transition. The structure property relationship between the alkyl chains, symmetrical structure, and linkage units serves as the main factor influencing the presence of mesophase.

Keywords: Liquid crystals; amide; nematic; alkyl chains; mesophase

Received: April 2025; Accepted: August 2025

Liquid crystals (LCs), also known as mesophases, are unique materials that exhibit long-range molecular orientational order like crystalline solids but lack long-range three-dimensional positional order, similar to liquids [1, 2]. This intermediate state between the crystalline solid and amorphous liquid phases allows LCs to exhibit both liquid-like properties (e.g., fluidity, droplet formation, and inability to support shear) and solid-like characteristics (e.g., anisotropy in optical, electrical, and magnetic properties) [3-5]. Liquid crystalline mesophases also often display a periodic molecular arrangement in one or more spatial directions, further highlighting their dual nature [6–8].

Liquid crystal materials comprise the core units, terminal units, and linkage units [9]. The properties of the terminal and core units and their combination determine all the optical and physical characteristics of liquid crystals, including viscosities, dielectric constants, elastic constants, absorption spectra, transition temperatures, the presence of mesophases, anisotropies, and optical nonlinearities [10-14]. The physical characteristics' reliance on the molecular components can be demonstrated by several general findings [15,16]. Schiff-based liquid crystals, for example, are often unstable. Although molecules like ester, azo, and azoxy are more stable, they are quite vulnerable to UV light, moisture, and temperature changes [17]. Generally, a liquid crystal can be classified as nematic, cholesteric, smectic, or columnar mesophase depending on how the molecules are arranged [18].

Symmetrical compounds typically exhibit higher melting points compared to their less symmetrical isomers [19]. Several studies have shown a correlation between a molecule's symmetry number (σ) and its melting temperature [20]. Symmetry appears to influence the transition from a crystalline solid to an isotropic liquid; however, it is still uncertain whether symmetry has a similar effect on other order-to-disorder transitions, such as the transformation from a solid to a liquid crystalline phase or from a liquid crystal to an isotropic liquid [21]. Voisin and his colleagues reported a series of dibenzophenazine derivatives to examine the differences in phase transitions among sixteen pairs of isomers with varied overall molecular symmetry. Their results indicated that molecular symmetry had a limited effect on the clearing temperature. However, in all but one case, the more symmetrical isomer exhibited a significantly higher melting point. Similar

†Paper presented at the 5th IKMPB Online Symposium: Sustainable Chemistry Innovations Shaping the Future Life

trends have been observed in discotic mesogens derived from triphenylene, where molecular symmetry shows a stronger influence on the clearing temperatures [22].

Symmetrical amide-based liquid crystals with different alkyl chains are characterized by their unique structural design and tunable mesophase behavior. These compounds feature a symmetric core with amide linkages that enhance intermolecular hydrogen bonding, leading to improved thermal stability and organized mesophase structures [23]. The incorporation of varying alkyl chain lengths on either side of the molecule allows for fine-tuning of molecular packing, flexibility, and overall mesophase characteristics, such as transition temperatures, type of mesophase (e.g., nematic, smectic), and temperature range of liquid crystalline phases [24]. This structural versatility makes them particularly attractive for developing advanced functional materials in optoelectronic applications [25]. The ability to tailor the physical properties through simple modifications in the alkyl chains sets these materials apart from traditional LC systems, marking a significant advancement in LC molecular design.

The ability to tailor properties through alkyl chain variation is closely linked to the presence of these chains, as liquid crystals rely on them to provide amphipathic characteristics, enabling solubility in both ionic and organic solvents [26]. However, the length of alkyl chain can affect the structure of the compound and hence influence the overall chemical compound [27]. For instance, for an organic surfactant compound, a higher alkyl chain length improves the packing of surfactant molecules at the metal-electrolyte interface, leading to a better inhibition performance; on the other hand, a very high hydrophobicity level reduces the inhibition performance [28]. The length of alkyl chain also has a significant effect on liquid crystals. Xu and colleagues examined the influence of alkyl chain length on the properties of 1-alkyl-3-methylimidazolium fluorohydrogenate ionic liquid crystals [29]. Their findings revealed a parallel increase of mesophase's temperature range with alkyl chain length. This is primarily due to the dissolution of van der Waals interactions between the alkyl chains, which is reflected in the rise in transition temperature, or ΔH, at clearing temperatures as alkyl chain length increases. The layer gap of the interdigitated bilayer structures increases in the crystalline phase and the liquid crystalline mesophase as the alkyl chain length increases. Due to the development of a smectic layer structure, the ionic conductivity of $C_xMIm(FH)_2F$ (x=12, 14, and 16) showed a notable anisotropy, and the anisotropy increases in degree as the cation's alkyl chain length increases [29].

While liquid crystal compounds have been the subject of much investigation, the phase characteristics of symmetrical amide-based molecules coupled to various terminal groups remain largely unexplored. There is a lack of research on the interaction between the terminal group, linking unit, and core system as a key factor in a compound's ability to exhibit the mesophase transition. Therefore, this research is focused on investigating the influence of varying alkyl chain lengths on the mesophase behavior exhibited by symmetrical amide-based liquid crystals. It examines the effect of alkyl side chain length variation on the thermal and structural characteristics of the resulting mesophases, thereby shedding light on the structure–property relationships within this class of compounds. This is achieved by introducing various terminal chains into the compounds to assess their influence on mesophase formation and other key properties. The purpose of varying the terminal chains is to influence the molecular interactions and structural alignment, which are essential for the development of liquid crystalline phases.

EXPERIMENTAL

Chemicals and Materials

The chemicals and solvents used in this study are 1-bromoheptane, 1-bromodecane, 1,4-phenylenediamine, methyl-4-hydroxybenzoate, potassium carbonate, potassium iodide, potassium hydroxide, thionyl chloride, dimethylformamide, dichloromethane, triethylamine, tetrahydrofuran, and n-hexane. These chemicals were purchased and used without purification from Acros Organics (Geel, Belgium), BDH laboratory (British Drug Houses) (Nichiryo, Japan), QREC (Asia) (Selangor, Malaysia), Merck (Darmstadt, Germany), and Sigma-Aldrich (Steinheim, Germany).

Characterization Methods

The examination of the synthesized compounds was twofold: spectroscopic analysis and liquid crystal investigation. The synthesized compounds were characterized using Fourier transform infrared (FTIR) spectroscopy of PerkinElmer FTIR Microscope Spotlight 200 spectrometer (PerkinElmer, Waltham, MA, USA) to identify the functional groups. Measurements were conducted via the attenuated total reflectance (ATR) technique over a wavenumber range of 500–4000 cm^{-1}. Nuclear magnetic resonance (NMR) spectroscopy (Bruker, Coventry, UK) was utilized to determine the molecular structures by examining the ^{1}H and ^{13}C nuclei. The NMR spectra were acquired on a Bruker 500 MHz Ultrashield spectrometer using DMSO-d_6 as deuterated solvents. Meanwhile, CHN elemental analysis was performed using PerkinElmer II, 2400 (PerkinElmer, Waltham, MA, USA) to evaluate the purity of the compounds by measuring the carbon (C), hydrogen (H), and nitrogen (N) content and comparing the experimental results. Polarized optical microscopy (POM) was also used to observe the phase textures of the samples by employing a system from Linkam (London, UK). Phase transitions were monitored during both heating and cooling cycles. A quantitative thermoanalytical technique known as differential scanning calorimetry

(DSC) was performed to further verify the mesophase transitions observed via POM. The samples were heated at a rate of 10 °C/min and held at their isotropic temperature for 2 minutes to ensure thermal stability. All DSC thermograms were recorded using a Pyris 1 Differential Scanning Calorimeter (PerkinElmer, Waltham, MA, USA).

Synthesis Summary

Intermediates **1a-b** were synthesized via the alkylation reaction of methyl-4-hydroxybenzoate and followed by the saponification reaction, as shown in Scheme 1 [30]. Next, intermediates **1a-b** underwent nucleophilic substitution reaction to form acyl chloride before reacting with 1,4-phenylenediamine to form the products, **2a-b**, as shown in Scheme 2 [31].

Synthesis of Intermediates 1a-b

Methyl-4-hydroxybenzoate (0.10 mol) and 1-bromoheptane (0.10 mol) were dissolved in DMF (20 mL) separately and mixed in a 100-mL round-bottom flask. Potassium carbonate (0.15 mol) and potassium iodide (0.01 mol) were added to the mixture and it was refluxed for 12 hours. Upon completion, the mixture was poured into cold water (300 mL). The precipitate formed was filtered and mixed with potassium hydroxide, KOH (0.20 mol), in ethanol (150 mL). The mixture was refluxed for 3 hours. The reaction progress was monitored by TLC. Next, the mixture was poured into water (300 mL) and a clear solution was formed. HCl was added to the solution and the mixture was stirred slowly until precipitate was formed. The precipitate was filtered, washed with water, and dried overnight to obtain a white powder. The same method was used to synthesize intermediate **1b**.

4-(heptyloxy)benzoic Acid, 1a

Yield = 10.01g (55.89%), mp: 105-107 °C, White brown precipitate. **FTIR (cm^{-1})**: 2927.04 and 2851.19 (Csp_3-H stretching), 1672.54 (C=O stretching) 1603.21 and 1429.46 (C=C benzene ring stretching), 1249.48 (C-O stretching). **^{1}H-NMR (500MHz, DMSO-d$_6$)** δ, ppm: 7.78 (d, J=5 Hz, 2H), 6.73 (d, J=10 Hz, 2H), 3.96 (t, J=10 Hz, 2H), 1.68 - 1.74 (m, 2H), 1.40 – 1.46 (m, 2H), 1.31 – 1.38 (m, 6H), 0.89 (t, J=15 Hz, 3H). **^{13}C-NMR (125MHz, DMSO-d$_6$)** δ, ppm: 168.78, 158.91, 135.20, 130.31, 112.80, 67.73, 40.61, 40.52, 40.44, 40.35, 40.28, 40.19, 40.11, 40.02, 39.85, 39.68, 39.52, 31.09, 28.83, 25.44, 21.82, 13.60. **CHN elemental analysis**: Calculated for $C_{14}H_{20}O_3$: C: 71.16%, H: 8.53%. Found: C: 71.11%, H: 8.50%.

4-(decyloxy)benzoic Acid, 1b

Yield: 10.00g (45.31%), mp: 104-106 °C, White brown precipitate. **FTIR (cm^{-1}):** 2917.44 and 2850.39 (Csp^3-H stretching), 1672.81 (C=O stretching), 1601.92 and 1429.46 (C=C stretching), 1250.18 (C-O stretching). **^{1}H-NMR (500MHz, DMSO-d$_6$)** δ, ppm: 7.78 (d, J=5 Hz, 2H), 6.73 (d, J=10 Hz, 2H), 3.96 (t, J=10 Hz, 2H), 1.68 - 1.73 (m, 2H), 1.40 – 1.46 (m, 2H), 1.29 – 1.36 (m, 12H), 0.87 (t, J=15 Hz, 3H). **^{13}C-NMR (125MHz, DMSO-d$_6$)** δ, ppm: 168.78, 159.00, 134.78, 130.36, 112.83, 67.73, 40.46, 40.37, 40.30, 40.21, 40.13, 39.96, 39.80, 39.63, 39.46, 31.13, 28.82, 28.79, 28.77, 28.62, 28.47, 25.45, 21.85, 13.60. **CHN elemental analysis**: Calculated for $C_{17}H_{26}O_3$: C: 73.35%, H: 9.41%. Found: C: 73.28%, H: 9.36%.

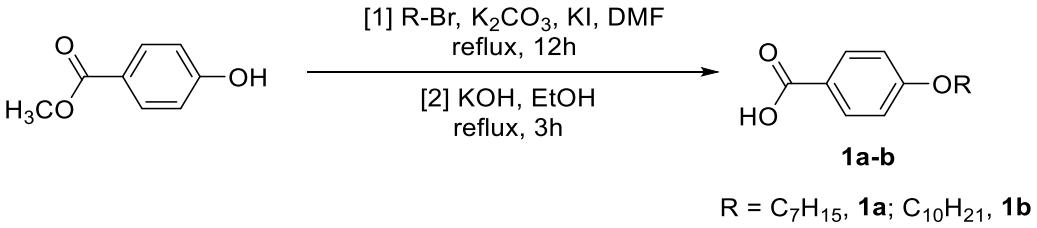

Scheme 1. Formation of intermediates **1a-b**.

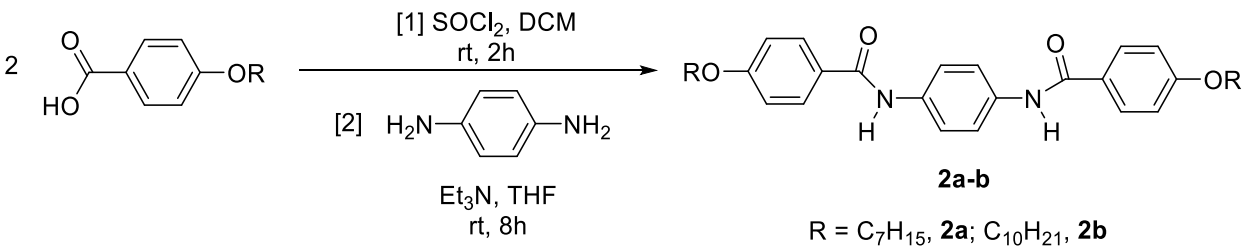

Scheme 2. Formation of compounds **2a-b**.

Synthesis of Compounds 2a-b

4-Heptyloxybenzoic acid, **1a** (0.06 mol) and thionyl chloride (0.06 mol) in DCM (40 mL) were mixed in a 100 mL round-bottom flask to form acid chloride. The mixture was stirred at room temperature for 2 hours to form a clear solution. A solution of 1,4-phenylenediamine (0.03 mol) in THF (20 mL) was added dropwise to the mixture and a white precipitate began to form. Triethylamine, Et_3N (0.03 mol) was added and the mixture was stirred for 8 hours. The reaction progress was monitored by TLC. The precipitate formed was filtered and the filtrate was collected. After it was dried, the product formed was recrystallized from methanol. This method was repeated to synthesize compound **2b**.

N,N'-(1,4-phenylene)bis(4-(heptyloxy)benzamide), 2a

Yield: 1.45g (96.67%), mp: 97-99 ℃, dark grey precipitate. **FTIR (cm^{-1}):** 2925.36 and 2854.47 (Csp^3-H stretching), 1655.64 (C=O stretching), 1604.21 and 1511.19 (C=C stretching), 1251.13 (C-O stretching). **^{1}H-NMR (500MHz, DMSO-d$_6$)** δ, ppm: 9.40 (s, 1H), 7.87 (d, J=10 Hz, 2H), 7.46 (s, 2H), 6.99 (d, J=5 Hz, 2H), 4.00 (t, J=10 Hz, 2H), 1.67 – 1.72 (m, 2H), 1.31 – 1.41 (m, 2H), 1.22 – 1.26 (m, 6H), 0.84 (t, J=10 Hz, 3H). **^{13}C-NMR (125MHz, DMSO-d$_6$)** δ, ppm: 165.56, 161.84, 154.13, 131.30, 129.68, 123.23, 115.69, 68.69, 40.52, 40.35, 40.18, 40.02, 39.85, 39.68, 39.52, 31.45, 29.00, 28.59, 25.75, 22.18, 13.94. **CHN elemental analysis**: Calculated for $C_{34}H_{44}N_2O_4$: C: 74.97%, H: 8.14%, N: 5.14%. Found: C: 74.95%, H: 8.12%, N: 5.10%.

N,N'-(1,4-phenylene)bis(4-(decyloxy)benzamide), 2b

Yield: 1.09g (72.83%), mp: 87-89 ℃, yellow precipitate. **FTIR (cm^{-1}):** 2915.31 and 2848.31 (Csp^3-H stretching), 1675.12 (C=O stretching), 1598.06 and 1467.95 (C=C stretching), 1295.12 (C-O stretching). **^{1}H-NMR (500MHz, DMSO-d$_6$)** δ, ppm: 9.24 (s, 1H), 7.90 (d, J=10 Hz, 2H), 7.48 (s, 2H), 7.01 (d, J=10 Hz, 2H), 4.03 (t, J=15 Hz, 2H), 1.69 - 1.75 (m, 2H), 1.38 – 1.44 (m, 2H), 1.25 – 1.33 (m, 12H), 0.85 (t, J=10 Hz, 3H). **^{13}C-NMR (125MHz, DMSO-d$_6$)** δ, ppm: 165.11, 161.80, 154.21, 131.54, 129.71, 123.00, 115.60, 68.65, 41.02, 40.85, 40.68, 40.52, 40.35, 40.18, 40.02, 31.62, 29.28, 29.24, 29.12, 29.07, 28.94, 28.87, 22.32, 14.03. **CHN elemental analysis**: Calculated for $C_{40}H_{56}N_2O_4$: C: 76.39%, H: 8.98%, N: 4.45%. Found: C: 76.33%, H: 8.82%, N: 4.41%.

RESULTS AND DISCUSSION

Summary of Physical Product Characteristics

Table 1 summarizes the product yield, melting point, and physical appearance of the synthesized intermediates (**1a–b**) and final compounds (**2a–b**). Yields are reported as percentages after purification. Yields below 60% were primarily attributed to factors such as incomplete reaction conversion, formation of side products, and material loss during purification steps.

Table 1. Summary of physical characteristics of the synthesized compounds.

Compound	Product Yield (%)	Melting Point (℃)	Physical Appearance
1a	55.89	105-107	White-Brown Precipitate
1b	45.31	104-106	White-Brown Precipitate
2a	96.67	97-99	Dark Grey Precipitate
2b	72.83	87-89	Yellow Precipitate

Table 2. Comparison of FTIR absorption bands of the synthesized compound with reported data.

Functional Group	Vibration Stretching (cm^{-1})		
	This Study	Abdul Rahim & Jamain (2025)	Jamain et al. (2020)
C-H sp^3 stretching	2851.07 and 2850.39	2931 and 2850	2919 and 2850
C=O stretching	1672	1669	1684
C=C stretching	1600	1606	1607
C-O stretching	1250	1254	1252

FTIR Spectral Discussion

The overall Fourier transform infrared spectra of intermediates **1a-b** displayed symmetrical or even asymmetrical C-H sp^3 absorption bands at 2851.07 and 2850.39 cm^{-1}. The C=O, C=C, and C-O stretching were attributed to the bands at 1672, 1600, and 1250 cm^{-1}, respectively. The absence of a large absorption band for the O-H stretching at 3100 cm^{-1} demonstrated the successful insertion of an alkyl group into the benzoate. These results are consistent with previous studies reported by Abdul Rahim & Jamain (2025) and Jamain et al. (2020), with slight differences in wavenumber (Table 2) [32,33].

Intermediates **1a** (heptyl chain) and **1b** (decanoyl chain) undergo reactions with $SOCl_2$ to produce acyl chloride intermediates. The acyl chlorides then react with 1,4-phenylenediamine to produce symmetrical amide-based compounds, **2a** (heptyl chain) and **2b** (decanoyl chain). Compounds **2a-b** show similar functional groups, with differences in the length of the respective alkyl chain. The peaks at 2915.31 and 2848.31 cm^{-1} were often formed by C-H sp^3 stretching, which exhibits significantly lower frequencies and is influenced by the compound's symmetrical stretching. Compared to the symmetric mode, the dipole mobility and intensity decrease in the symmetrical mode [34]. Furthermore, the existence of many CH_3 groups connected to the carbon will cause a peak split in the C-H sp^3 bending, which can be impacted within the region of 1370 to 1465 cm^{-1}. The FTIR spectrum observation reveals a prominent peak presence that typically appears at a wavenumber of 2915 cm^{-1} and is impacted by the absorption of C-H sp^3 in alkanes.

By examining the faint peaks at wavenumbers of 1370 to 1465 cm^{-1}, the FTIR spectrum also demonstrates the development of methyl groups, which can be identified as the presence of bending on CH_2 and symmetrical CH_3, respectively, in the alkyl chain inside the compounds. In the range of 1460 cm^{-1}, the symmetrical CH_3 bending deformation was seen close to the CH_2 value, with often overlapping and unresolved peaks. Consequently, the appearance areas of the absorption spectra were used to establish the presence of alkane groups in the compounds. The data spectrum also reveals the existence of a C-O band, which indicates the formation of ether at 1295.12 cm^{-1} for the final compound **2b**. The values of this compound may be somewhat different from those of compound **2a** or the same, depending on the length of structure construction.

Aromatic rings typically produce C=C stretching bands at a range value of appearance between 1450 and 1600 cm^{-1}. These bands are typically present in sharp bands at 1600, 1500, and 1475 cm^{-1}. A few peaks that formed in the intermediates of the FTIR spectrum indicated the presence of a benzene ring. When determining the substitution formation on the aromatic ring, it is often necessary to generate the C-H bends that are out-of-plane at a low wavenumber by examining the existence or lack of a ring-bending mode about 690 cm^{-1}. This means that strong bands in a range of 830 to 860 cm^{-1} may be used to interpret the out-of-plane and aromatic ring-bending modes, respectively. Subsequently, the two bands indirectly show that all the compounds have para-disubstituted, where 1,4-disubstituted ring is in the structural formation.

Although compounds **2a-b** consist of N-H stretching, which supposedly presents a sharp peak at the 3300 – 3000 cm^{-1} region, no peak is observed within that region in Figure 1. The absence of the N–H stretching peak in the FTIR spectrum may be attributed to the cancellation of the dipole moment within the molecule. This typically occurs when the N–H bond participates in a symmetrical molecular environment, where the stretching vibration does not result in a net change in the dipole moment. FTIR spectroscopy relies on changes in dipole moment during molecular vibrations to detect functional groups. Vibrations that do not produce such changes, particularly symmetric stretches, may become IR inactive or exhibit significantly reduced intensity. Consequently, the N–H bond, although present, may not produce a detectable peak under these conditions [35].

Table 3 presents a summary of the FTIR data for the final compounds. All the main absorption peaks were clearly observed in the FTIR spectra, corresponding to the expected functional groups present in the target compounds. These spectral features confirm that compounds **2a-b** were successfully synthesized as the characteristic vibrations, such as those associated with the carbonyl (C=O), amide (N–H), and alkyl (C–H) groups, were consistent with the proposed molecular structures. The presence of these key peaks provides strong evidence for the formation of the desired products and supports the structural integrity of the synthesized compounds.

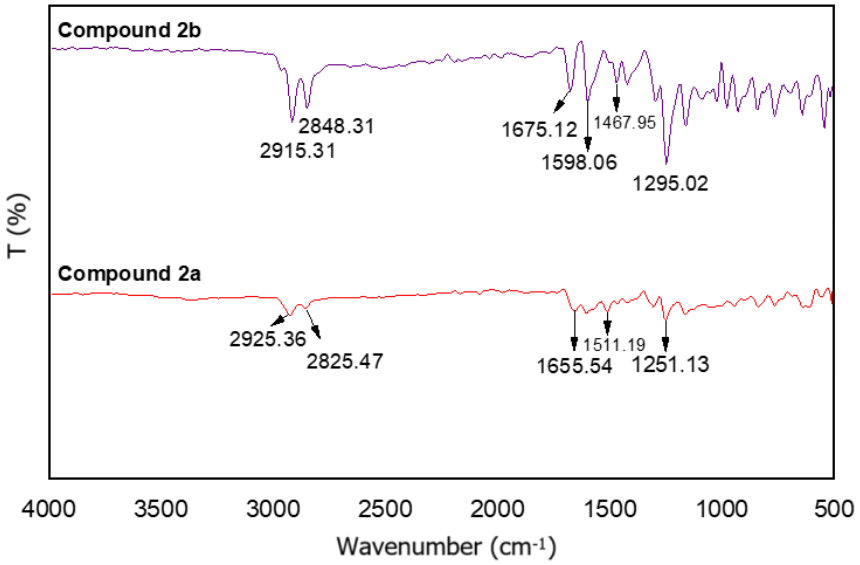

Figure 1. The overlay FTIR spectra of compounds **2a** and **2b**.

Table 3. FTIR vibrational stretching (cm^{-1}) for the synthesized compounds.

Compound	Vibration Stretching (cm^{-1})						
	N-H	NH_2	O-H	C_{sp3}-H	C=O	C=C	C-O
2a	-	-	-	2925.36 2854.47	1655.64	1604.21 1511.19	1251.13
2b	-	-	-	2915.31 2848.31	1675.12	1598.06 1467.95	1295.12

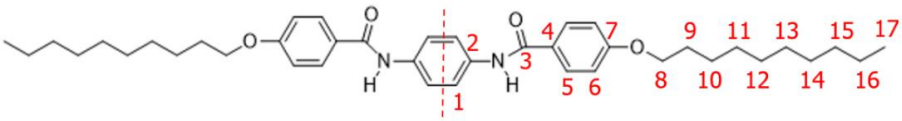

Figure 2. Chemical structure of compound **2b** with complete atomic numbering.

NMR Spectral Discussion

Since compounds **2a-b** are symmetrical compounds, a vertical plane of symmetry was induced to the center of the benzene ring to reduce the number of peaks. Compound **2b** was used as a representative for homologues. Figure 2 shows the chemical structure of compound **2b** with complete atomic numbering.

In the ^{1}H NMR spectrum (Figure 3), the downfield region at δ 9.24 ppm shows the presence of amino groups in the compound, indicating the successful formation of amide base. At the region of δ 7.00 – 7.91 ppm, the signals were assigned to significant aromatic protons like Ar-H. The aromatic protons were present in the downfield region due to the strong electron delocalization between them [36]. The chemical shift of H5 is higher than H6 since it is nearer than the electron-withdrawing group (i.e., amide group). The triplet proton signal at δ 4.03 ppm (H8) is noticeable as the O-CH_2 group. The next carbon atom in an alkyl chain can be found at the chemical shifts of δ 1.69 – 1.75 ppm (H9) and δ 1.38 – 1.44 ppm (H10). The remaining proton in the alkyl chains appeared in the region of δ 1.25 – 1.33 ppm (H11 – H16). Lastly, the signal at δ 0.85 ppm (H17) was assigned to the methyl proton. The chemical shifts observed in the aliphatic region of this compound closely resemble those reported by Jamain et al. (2025), indicating strong consistency in the aliphatic structural features and confirming the reliability of the spectral data [37].

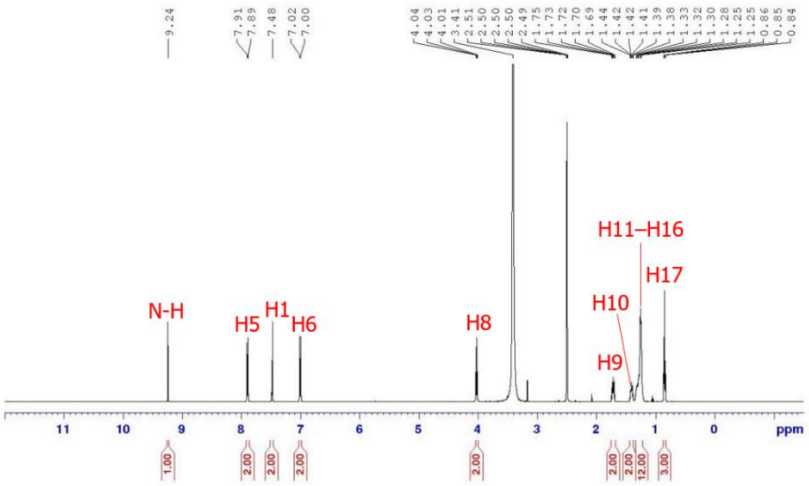

Figure 3. [1]H NMR spectrum of compound **2b.**

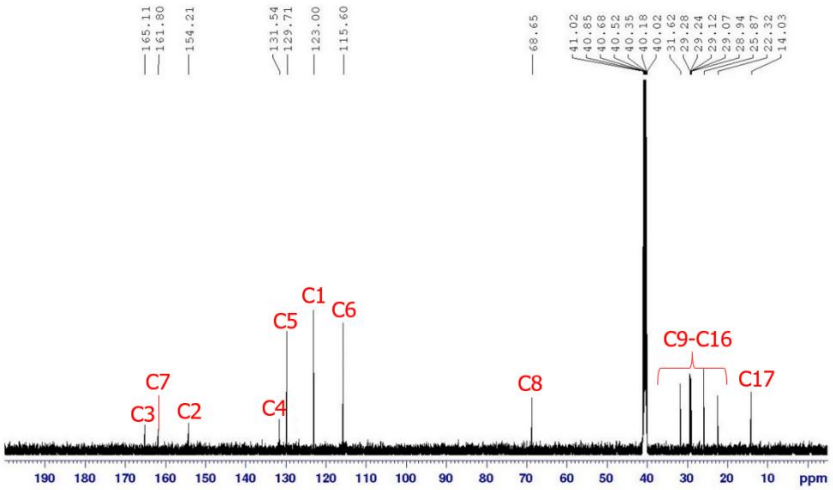

Figure 4. [13]C NMR spectrum of compound **2b**.

The carbon signal at δ 165.11 ppm in Figure 4 is identified as C3 due to its connection to the electronegative nitrogen and oxygen atoms. Owing to its attachment to the electronegative nitrogen atom, C2 is given at δ 161.80 ppm. Since the carbon signal at δ 154.21 ppm is bonded to the oxygen atom, it was designated as C7. Aromatic carbons were suggested by signals found in the δ 115.60 – 131.54 ppm range. The deshielded effect was prompted by sp2 hybridization and diamagnetic anisotropy in the carbon sheet [38]. Adding the NOE impact to this condition yields the development of peak intensity from the two carbon equivalents combined [39]. Signals seen at the highest field area in the spectrum are often composed of more shielded carbon. The highest intensity of carbon atoms linked to the alkyl chain was reported in the area between δ 14.03 and 31.62 ppm.

The NMR spectra of compound **2a** exhibited a pattern similar to that of compound **2b**, with slight variations observed particularly in the upfield region of the aliphatic range. This difference is attributed to the shorter alkyl chain in **2a**. Based on both the [1]H and [13]C NMR spectra of compound **2b**, the integration values matched the expected proton ratios, providing strong support for the proposed molecular structure and confirming the successful synthesis of the target compound.

CHN Elemental Analysis

Table 4 summarizes the percentages of carbon (C), hydrogen (H), and nitrogen (N) in intermediates **1a–b** and compounds **2a–b**. The percentage mistakes of each compound were determined to be fewer than 1%, indicating their purity.

Table 4. Summary of CHN elemental analysis data for all compounds.

Compound	%Found (Calculated)		
	C (%)	H (%)	N (%)
1a	71.11 (71.16)	8.50 (8.53)	-
1b	73.28 (73.35)	9.36 (9.41)	-
2a	74.95 (74.97)	8.12 (8.14)	5.10 (5.14)
2b	76.33 (76.39)	8.82 (8.98)	4.41 (4.45)

Table 5. The phase transition of compounds **2a-b**.

Compound	Mode	Transition Temperature (°C)				
2a	**Heating**	**Cr**		**N**		**I**
		•	98.4	•	152.9	•
	Cooling	**I**		**N**		**Cr**
		•	151.6	•	97.5	•
2b	**Heating**	**Cr**		**N**		**I**
		•	88.7		150.6	•
	Cooling	**I**		**N**		**Cr**
		•	148.7	•	86.3	•

Note: **Cr**=Crystal, **N**=Nematic, **I**=Isotropic

Determination of Liquid Crystal Properties by POM

The mesophase behavior of all compounds was determined using a polarized optical microscope (POM) through the heating and cooling rates of 5 °C. Compounds **2a-b** displayed liquid crystal mesophase and thus were referred to as mesogenic. Table 5 shows the mesophase characteristics of compounds **2a-b** under POM after the heating and cooling cycles.

Compound **2a** exhibited nematic phases in both the heating and cooling cycles. During the heating cycle, a nematic phase appeared at 98.4 °C before transitioning to the isotropic phase at 152.9 °C. In the cooling cycle, the compound displayed a nematic phase at 97.5 °C and crystallized at 151.6 °C. Similarly, compound **2b** also showed nematic phases in both thermal cycles. It exhibited a nematic phase at 88.7 °C during heating, followed by a transition to the isotropic phase at 148.7 °C. Upon cooling, the nematic phase reappeared at 151.6 °C before crystallizing at 86.3 °C.

Generally, all the nematic phases are fluid and have marbled textures, like those of a nematic phase of calamitic molecules, and characteristic schlieren textures with two and four brush defects [40]. Schlieren textures result from a typically constant shift in the orientation of the sample's optical index ellipsoid, which reflects a constant shift in the molecules' orientation [41]. The Schlieren textures of compounds **2a-b** are shown in Figure 5. Both compounds exhibit four black brushes, also known as four-point singularities. These singularity brushes rotate in the same direction as the polarizers, while the remaining brushes rotate in the opposite direction. Both the polarizers and brushes rotate at approximately the same rate [42].

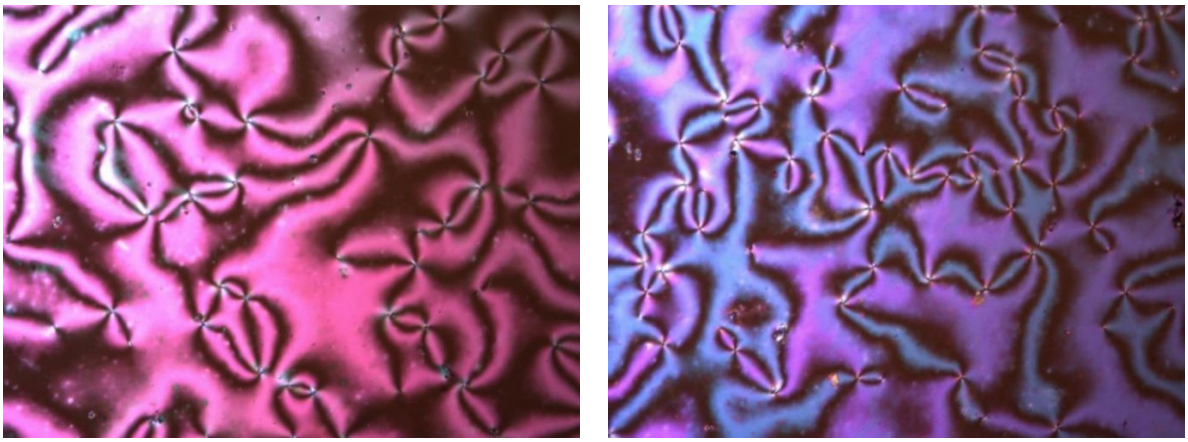

Figure 5. The POM photographs of the nematic of (a) compound **2a** and (b) compound **2b** upon the cooling cycle with a magnification of 20 × 0.50.

Conformation of Liquid Crystal Properties using DSC

The DSC thermogram of compound **2a** was used as a representation of other homologues. Figure 6 shows the phase transition of nematic's mesophase formation after the heating or cooling cycles.

There were two discernible peaks in the heating cycle. The first endotherm was recorded at 98.42 °C (2.3056 kJmol^{-1}), indicating the transition from crystal to nematic. As the heating process continued, isotropic phases developed at 152.92 °C (2.0551 kJmol^{-1}). The intermolecular interactions between molecules broke as a result of the development of all these peaks, and the endothermic energy was absorbed by the crystal molecules [43]. According to enthalpy observations, the crystal to nematic phase transition changes more than the nematic to isotropic phase transition. This phenomenon is caused by the fact that less latent heat is required to change a liquid crystal into a liquid than a solid crystal into a liquid. Furthermore, liquid crystal properties are more similar to that of liquid [44].

Similarly, two peaks occurred throughout the cooling cycle. Crystal formation started at 97.47 °C (-2.3181 kJmol^{-1}) after the transition from isotropic to nematic at 151.66 °C (-2.852 kJmol^{-1}). Exothermic energy was present during all of the transitional stages. Any energy released to establish an intermolecular link is known as exothermic energy. The isotropic to nematic phase transition had the largest enthalpy energy shift because sufficient energy must be released to generate a fully formed crystalline arrangement with strong intermolecular interactions [45].

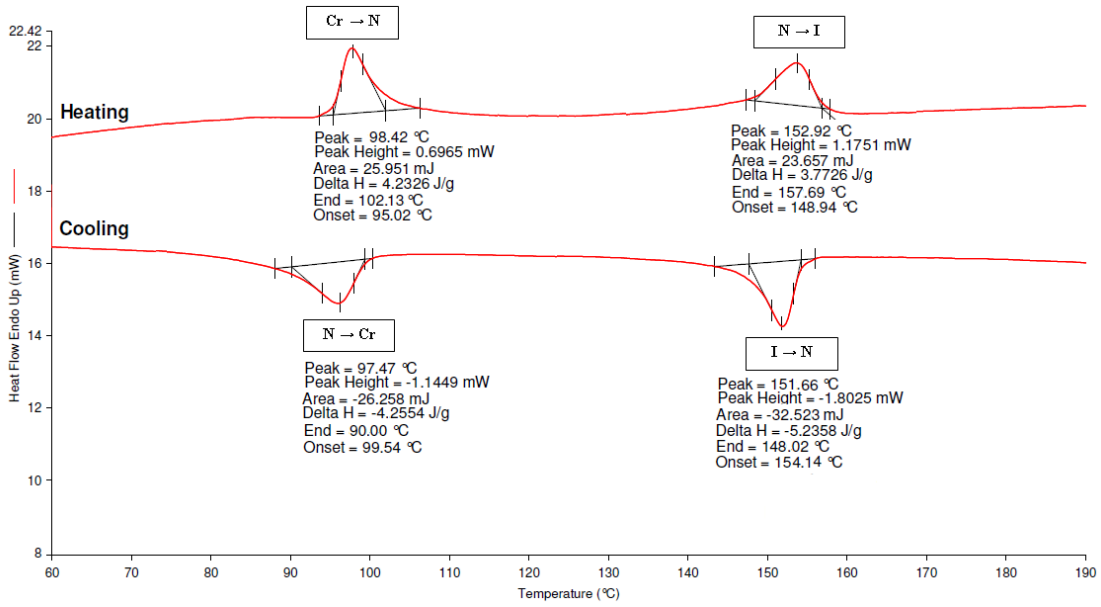

Figure 6. DSC thermogram of compound **2a**.

Structure Property Relationship

A liquid crystal comprises a core mesogen unit and a long alkyl chain connected with a linking unit. The relative ordering of the anions around the cations is influenced by the rotational flexibility over the bond between the ring and the alkyl chain, which has a significant impact on the melting enthalpy and entropy [46]. Hence, the rotational flexibility of the alkyl chain may have an impact on the melting point of liquid crystal. A saturated alkyl chain is said to be more flexible than an unsaturated alkyl chain due to the presence of pi electron in unsaturated alkyl chain [47].

Several studies suggest that because heteroatoms (S, O, and N) may dramatically alter molecular geometric structure, polarity, and polarizability, heterocyclic rings in the stiff central core of liquid crystalline molecules may transmit changes in the mesophases and physical characteristics [48-50]. An efficient method of expanding the liquid crystal phase interval is the introduction of $\boldsymbol{\pi}$-conjugation units to improve the molecular anisotropies by enhancing the intermolecular actions, such as intermolecular $\boldsymbol{\pi}$-$\boldsymbol{\pi}$ stacking and dipole-dipole actions. However, a moderate intermolecular action is favorable for the liquid crystal phase stability [51]. In this research, the conjugation between the aromatic rings with the amide linkage unit strengthens the intermolecular and intramolecular interactions and leads to the synthesis of a stable amide-based liquid crystalline.

Table 6 presents a comparative summary of amide-based liquid crystals reported in the literature, highlighting the influence of alkyl chain length and amide linkages on mesophase behavior. Shorter chains generally exhibit lower transition temperatures and less ordered phases, while longer chains promote higher melting points and smectic ordering [52]. The presence of multiple amide linkages typically enhances intermolecular hydrogen bonding, leading to increased thermal stability [53]. The data from this study are included for a direct comparison with previously reported systems.

It is widely accepted that when the number of aromatic rings in the mesogenic unit of liquid crystalline compounds increases the resonance and concurrent polarisation, thus making it more planar in shape, the degree of thermal transformation of the liquid crystalline and isotropic phases is somewhat higher [56]. The presence of more aromatic rings in the liquid crystal will boost the degree of thermal transformation of the liquid crystalline, hence causing the melting point to rise [57]. In this research, both compounds consist of 3 aromatic rings, resulting in an extremely high melting temperature (T_m) at 98 °C.

The symmetrical structure of both compounds also contributes to improved efficiency in the crystalline phase, leading to a further increase in lattice energy [58]. More energy is needed to break the intermolecular bond and lattice energy, thus raising the melting point. Donaldson and his colleagues found that while the equivalent non-symmetric dimers do display smectic behavior, the symmetric dimers only exhibit nematic behavior [59]. A symmetrical liquid crystal usually will exhibit a nematic phase since a symmetrical compound often consists of an axis of symmetry to produce superimposed mirror image [60]. This is similar to the nematic phase, which contains a director throughout the medium. Besides, symmetrical molecules are considered nonpolar while asymmetrical molecules are considered polar due to their lopsided charge distribution. The intermolecular bonds in asymmetrical molecules can be higher in number and stronger than symmetrical molecules based on the difference in polarity [61]. The interpretation for the formation of smectic phases in non-symmetric dimers containing cholesteryl is a delicate equilibrium of the van der Waals interactions between the cholesteryl segment and other aliphatic chains and the electrostatic interactions between the cholesteryl and aromatic-based units [62]. In this research, compounds **2a-b,** which are symmetrical amide-based liquid crystals, exhibit only the nematic phase.

Table 6. Comparative data for amide-based liquid crystals from the literature.

Compound Structure	Alkyl Chain Length	Amide Linkage (s)	Mesophase Type	Ref.
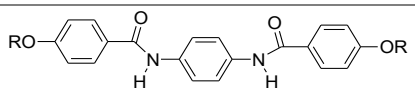 **2a-b** R = C_7H_{15}, **2a**; $C_{10}H_{21}$, **2b**	C7 and C10	2	Nematic	This Study
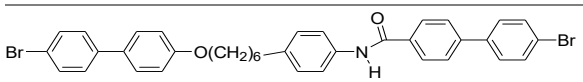	C6 (Spacer)	1	Nematic	[54]
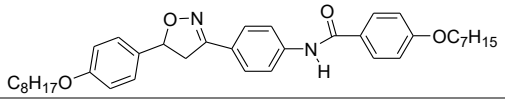	C7 and C8	1	Smectic A and C	[55]

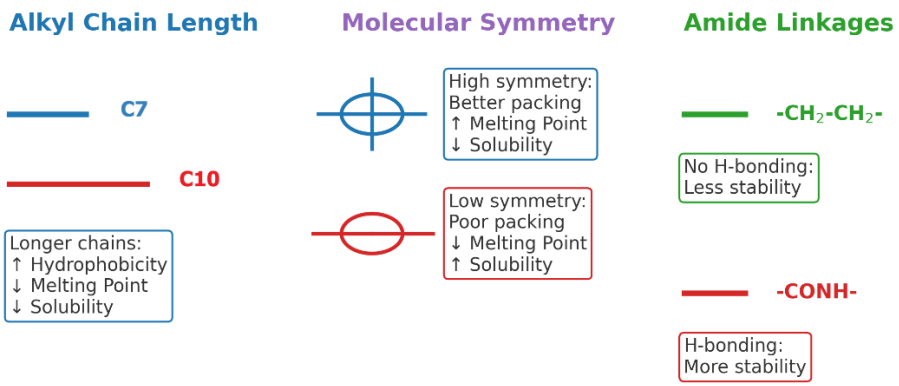

Figure 7. Effects of alkyl chain length, symmetry, and amide linkages on phase behavior.

Compounds **2a-b** possess relatively high melting points. This is primarily due to the presence of strong intermolecular interactions, including hydrogen bonding and van der Waals forces, inherent to amide-containing structures. A significant amount of energy is required to overcome these interactions, resulting in elevated melting temperatures [63]. Furthermore, the rigid, linear structure of the molecules allows for efficient van der Waals packing, which enhances molecular order and stability in the solid phase. However, this packing comes at the expense of rotational flexibility, which is typically observed in mesogenic units with more flexible linkages. The reduced rotational flexibility contributes further to the increased thermal stability, thereby raising the melting point [64]. Past research suggests that compound **2b** should exhibit nematic phase at a higher temperature compared to compound **2a** since it has longer alkyl chain and higher energy required to break the intermolecular bond. However, compound **2b** had a lower melting point (88.65 ℃) than compound **2a** (98.42 ℃). Since both compounds consist of long alkyl chains, the lower melting point may be due to increased rotational flexibility. These findings are consistent with those of Strachan et al. (2021), who reported similar nematic behavior in amide-based compounds with different alkyl chains [54]. The relative ordering of the anions around the cations is influenced by the rotational flexibility over the bond between the ring and the alkyl chain, which has a significant impact on the melting enthalpy and entropy [65, 66]. The visual diagrams in Figure 7 show the effects of alkyl chain length, symmetry, and amide linkages on phase behavior.

CONCLUSION

In conclusion, all the intermediates and compounds were successfully characterized using FTIR, NMR spectroscopy, and CHN elemental analysis. The FTIR spectra clearly demonstrated the presence of amide linkages, with the characteristic C=O stretching observed at 1700 cm^{-1}. In the ^{1}H NMR data, a singlet peak at δ 9.24 ppm confirmed the presence of amino groups, indicating successful formation of the amide base. Additionally, CHN elemental analysis showed less than 1% error for all compounds, confirming their high purity. The liquid crystal mesophase behavior was determined using polarized optical microscopy (POM), where compounds **2a-b** exhibited nematic phases, establishing that these symmetrical amide-based liquid crystals display exclusively nematic behavior. The incorporation of long alkyl chains contributed to increased molecular flexibility and stabilized intermolecular interactions essential for mesophase formation. Furthermore, the conjugation between the aromatic ring and amide linkage resulted in an increased melting temperature (T_m), as supported by thermal transitions observed via DSC thermograms. This study represents one of the first demonstrations of symmetrical amide-based liquid crystals featuring both heptyl ($-C_7H_{15}$) and decyl ($-C_{10}H_{21}$) alkyl chains exhibiting nematic phases. These findings highlight the potential to tune mesophase temperature ranges through alkyl chain length variation, providing valuable insights for designing liquid crystalline materials with tailored properties. Such structural-property relationships pave the way for future applications of these materials in advanced technologies such as display devices and chemical sensors, where precise control over mesophase behavior is critical.

ACKNOWLEDGEMENTS

The authors wish to acknowledge the funding received from Universiti Malaysia Sabah (Grant Number GKP2407 and SPB0004-2020) and the lab facility support from Universiti Sains Malaysia.

The authors declare that they have no conflict of interest.

REFERENCES

1. Goossens, K., Lava, K., Bielawski, C. W. and Binnemans, K. (2016) Ionic Liquid Crystals: Versatile Materials. *Chemical Reviews*, **116**, 4643–4807.

2. Andrienko, D. (2018) Introduction to Liquid Crystals. *Journal of Molecular Liquids*, **267**, 520–541.

3. Levine, A. W. (1975) Structure-Property Relationships in Thermotropic Organic Liquid Crystals. In: Priestley, E. B., Wojtowicz, P. J., Sheng, P. (eds) Introduction to Liquid Crystals. *Springer, Boston, MA*.

4. Lagerwall, J. P. F. and Scalia, G. (2012) A New Era for Liquid Crystal Research: Applications of Liquid Crystals on Soft Matter Nano-, Bio- and Microtechnology. *Current Applied Physics*, **12**, 1387–1412.

5. Habil, S., Jamain, Z. and Makmud, M. Z. H. (2024) Synthesis and Characterization of Azo-Based Cyclotriphosphazene Compounds: Liquid Crystalline and Dielectric Properties. *ChemEngineering*, **8**, 71.

6. Guardià, J., Reina, J. A., Giamberini, M. and Montané, X. (2024) An Up-to-Date Overview of Liquid Crystals and Liquid Crystal Polymers for Different Applications: A Review. *Polymers*, **16**, 2293.

7. Joshi, V. K., Katariya, K. D. and Nakum, K. J. (2024) Synthesis, Mesomorphic Behaviour, and DFT Studies of Biphenyl Bis-Ester Schiff Base Liquid Crystals. *Journal of Molecular Structure*, **1311**, 138338.

8. Singh, S. and Dunmur, D. A. (2002) Liquid Crystals: Fundamentals. *Danvers: World Scientific Publishing Co. Pte. Ltd.*

9. Jamain, Z., Azman, A. N. A., Razali, N. A. and Makmud, M. Z. H. (2022) A Review on Mesophase and Physical Properties of Cyclotriphosphazene Derivatives with Schiff Base Linkage. *Crystals*, **12**, 1174.

10. Nawawi, M. F., Salleh, N. M., Lee, V. S. and Cheng, S. -F. (2023) Synthesis, Characterization and Structure-Mesomorphic Properties Relationship of Palm-Based Azo-Ester Bridged Liquid Crystals from Caprylic Acid. *Industrial Crops and Products*, **199**, 116765.

11. Jamain, Z. Habil, S. Makmud, M. Z. H. and Khairuddean, M. (2021) Synthesis, Structural and Dielectric Characteristics of Liquid Crystalline Azo-Based Compounds with Different Terminal Length. *In Proceedings of the 2021 IEEE International Conference on the Properties and Applications of Dielectric Materials (ICPADM), Johor Bahru, Malaysia*, 49–52, 12–14 July 2021.

12. Smith, C. (2018) A Review of Liquid Crystal Display Technologies, Electronic Interconnection and Failure Analysis. *Circuit World*, **34**, 35–41.

13. Jevtovic, V., Ahmed, H. A., Khan, M. T., Al Zahrani, S. A., Masood, N. and Jeilani, Y. A. (2023) Preparation of Laterally Chloro-Substituted Schiff Base Ester Liquid Crystals: Mesomorphic and Optical Properties. *Crystals*, **13**, 835.

14. Jamain, Z., Khairuddean, M. and Saidin, S. A. (2019) Synthesis and Characterisation of 1,4-Phenylenediamine Derivatives Containing Hydroxyl and Cyclotriphosphazene as Terminal Group. *Journal of Molecular Structure*, **1186**, 293–302.

15. Bian, X. C., Chen, L., Wang, J. S. and Wang, Y. Z. (2010) A Novel Thermotropic Liquid Crystalline Copolyester Containing Phosphorus and Aromatic Ether Moiety Toward High Flame Retardancy and Low Mesophase Temperature. *Journal of Polymer Science Part A: Polymer Chemistry*, **48**, 1182–1189.

16. Khoo, I. C. (2007) Liquid Crystals, 2nd ed. *John Wiley & Sons, Inc.: Hoboken, NJ, USA*, 60–65.

17. Ge, Z. X., Wang, Y. M., Sun, J. T., Zhang, Z. Y., Jia, Y. G., Tian, M. and Yao, D. S. (2023) Novel Starshaped Liquid Crystal Macromolecules Based on Conjugated Structures of Azo and Schiff Bases: Synthesis and Properties. *Liquid Crystals*, **50**, 2413–2433.

18. Collings, P. J. (2002) Liquid Crystals: Nature's Delicate Phase of Matter. *Princeton University Press, Princeton, NJ, USA*.

19. Brown, R. J. C. and Brown, R. F. C. (2000) Melting Point and Molecular Symmetry. *Journal of Chemical Education*, **77**, 724.

20. Pinal, R. (2004) Effect of Molecular Symmetry on Melting Temperature and Solubility. *Organic & Biomolecular Chemistry*, **2**, 2692.

21. Ishihara, S. and Uto, S. (2023) Symmetry and Liquid Crystals. *Symmetry*, **15**, 691.

22. Voisin, E., Johan Foster, E., Rakotomalala, M. and Williams, V. E. (2009) Effects of Symmetry on the Stability of Columnar Liquid Crystals. *Chemistry of Materials*, **21**, 3251–3261.

23. Romo-Uribe, A. and Maranzano, B. J. (2024) On the Structure and Thermo-Mechanical Properties of a Thermotropic Liquid Crystalline Copolyester Amide. *Polymer*, **301**, 27026.

24. Strachan, G. J., Zattarin, A., Storey J. M. D. and Imrie, C. T. (2023) Tailoring Amide N-Substitution to Direct Liquid Crystallinity in Benzanilide-Based Dimers. *Journal of Molecular Liquids*, **384**, 122160.

25. Neto, J. L, da Silva, L. P. A, da Silva, J. B., Ferreira, R. L., da Silva, A. J. C., da Silva, J. C. S., de Oliveira, Í. N., Lima, D. J. P. and Ribeiro, A. S. (2021) Multielectrochromic Amide-Based Poly (2,5-Dithienylpyrrole) Bearing A Fluorene Derivative: Synthesis, Characterization, and Optoelectronic Properties. *Electrochimica. Acta*, **379**, 138173.

26. Mohram, S., Jamain, Z. and Khairuddean, M. (2025) Synthesis and Characterization of Non-Mesogenic Amide-Ester Derivatives Containing Different Terminal Alkyl Chains. *Malaysian Journal of Chemistry*, **27**, 184–196.

27. Sharma, V. S. and Patel, R. B. (2016) Molecular Structure and Mesomorphism: Effect of Tail/ Lateral Group. *Molecular Crystals and Liquid Crystals*, **630**, 58–68.

28. Verma, C., Quraishi, M. A. and Rhee, K. Y. (2022) Hydrophilicity and Hydrophobicity Consideration of Organic Surfactant Compounds: Effect of Alkyl Chain Length on Corrosion Protection. *Advances in Colloid and Interface Science*, **306**, 102723.

29. Xu, F., Matsumoto, K. and Hagiwara, R. (2010) Effects of Alkyl Chain Length on Properties of 1-Alkyl-3-methylimidazolium Fluorohydrogenate Ionic Liquid Crystals. *Chemistry – A European Journal*, **16**, 12970–12976.

30. Usri, S. N. K., Jamain, Z. and Makmud, M. Z. H. (2022) Fire Retardancy and Dielectric Strength of Cyclotriphosphazene Compounds with Schiff Base and Ester Linking Units Attached to the Electron-Withdrawing Side Arm. *Polymers*, **14**, 4378.

31. Mohamad Fazli, F. J. and Jamain, Z. (2024) Synthesis and Characterization of Hydrazine Bridge Cyclotriphosphazene Derivatives with Amide–Schiff Base Linkages Attached to Decyl and Hydroxy Terminal Groups. *Molbank*, **2024**, M1934.

32. Abdul Rahim, K. and Jamain, Z. (2025) Synthesis and Characterization of Amide-Based Cyclotriphosphazene Derivatives with Alkoxy Terminal Groups. *Molbank*, **2025**, M2039.

33. Jamain, Z., Khairuddean, M. and Guan-Seng, T. (2020) Synthesis of Novel Liquid Crystalline and Fire Retardant Molecules Based on Six-Armed Cyclotriphosphazene Core Containing Schiff Base and Amide Linking Units. *RSC Advances*, **10**, 28918–28934.

34. Pavia, D. L., Lampman, G. M., Kriz, G. S. and Vyvyan, J. R. (2009) Introduction to Spectroscopy (4th ed.). *Brooks/Cole Cengage Learning*.

35. Waldin, N. A. and Jamain, Z. (2023) Synthesis and Mechanical Property of Hexasubstituted Cyclotriphosphazene Derivatives Attached to Hydrazine-Bridge Linkage with High Fire Retardancy. *Journal of Molecular Structure*, **1284**, 135330.

36. Rajkumar, P., Selvaraj, S., Anthoniammal, P., Ram Kumar, A., Kasthuri, K. and Kumaresan, S. (2023) Structural (Monomer and Dimer), Spectroscopic (FT-IR, FT-Raman, UV–Vis and NMR) and Solvent Effect (Polar and Nonpolar) Studies of 2-Methoxy-4-Vinyl Phenol. *Chemical Physics Impact*, **7**, 100257.

37. Usri, S. N. K., Jamain, Z. and Makmud, M. Z. H. (2025) Synthesis and Molecular Elucidation of New Hexasubstituted Cyclotriphosphazene Derivatives: Determination on Flame Retardancy, Thermal Behavior and Dielectric Properties. *Journal of Molecular Structure*, **1328**, 141349,

38. Waldin, N. A. and Jamain, Z. (2023) The Effect of Alkyl Terminal Chain Length of Schiff-Based Cyclotriphosphazene Derivatives Towards Epoxy Resins on Flame Retardancy and Mechanical Properties. *Polymers*, **15**, 1431.

39. Kara, Y. S. and Diran, D. (2024) Synthesis of Novel 1,2,4-Oxadiazine Derivatives and The Substituent Effect Study on ^{13}C NMR Spectra. *Journal of Molecular Structure*, **1310**, 138309.

40. Bisoyi, H. K. and Kumar, S. (2010) Discotic Nematic Liquid Crystals: Science and Technology. *Chemical Society Reviews*, **39**, 264–285.

41. Nehring, J. and Saupe, A. (1972) On the Schlieren Texture in Nematic and Smectic Liquid Crystals. *Journal of the Chemical Society, Faraday Transactions 2*, **68**, 1–15.

42. Mali, A. A. A. and Jamain, Z. (2023) Synthesis and Characterization of Non-Mesogenic Behavior of Chalcone Derivatives. *Malaysian Journal of Chemistry*, **25**, 158–168.

43. Sulaiman, N. I., Abu Bakar, N. H. H. and Abu Bakar, M. (2024) Effect of Al-doping on Structural and Adsorption Properties of $NiFe_2O_4$ via Modified Sol–Gel Approach for CO_2 Adsorption. *Chemistry Africa*, **7**, 2139–2154.

44. Jamain, Z. and Khairuddean, M. (2021) Synthesis and Mesophase Behaviour of Benzylidene-Based Molecules Containing Two Azomethine Units. *Journal of Physics: Conference Series*, **1882**, 012120.

45. Karanlık, G., Ocak, H. and Bilgin Eran, B. (2019) Imine Based Chiral Liquid Crystals: Effect of Varying The Terminal Substituent and Orientation of Ester Linking Unit. *Journal of Molecular Liquids*, **275**, 567–577.

46. Jamain, Z., Khairuddean, M., Zulbaharen, N. N. and Chung, T. K. (2019) Synthesis, Characterization and Determination of Mesophase Transition of Azo-Azomethine Derivatives with Different Terminal Chain Lengths. *Malaysian Journal of Chemistry*, **21**, 73–85.

47. Lee, W. N., Salleh, N. M., Velayutham, T. S. and Cheng, S. F. (2023) Synthesis, Phase Transition Behaviour and Dielectric Properties of Smectogenic Palm-Based Liquid Crystals Containing Schiff Base Ester and Phenyl Ring. *Journal of Molecular Structure*, **1282**, 135168.

48. Zulaziz, N. A. S., Jamain, Z. and Khairuddean, M. (2024) Synthesis, Characterization, and Liquid Crystalline Behavior of Ester-Schiff Base Derivatives Attached to Nonyl and Tetradecyl Terminal Chains. *Malaysian Journal of Chemistry*, **26**, 572–582.

49. Valadbeigi, Y. (2018) Comparison of Effects of Charge Delocalization and Π-Electron Delocalization on The Stability of Monocyclic Compounds. *Journal of Molecular Graphics and Modelling*, **80**, 104–112.

50. Fadhil, M. Z. A. M., Mustamin, M. A. and Jamain, Z. (2024) Liquid Crystalline Behaviour of Symmetrical Thermotropic Schiff Base Compounds. *Journal of Molecular Structure*, **1315**, 138929.

51. Chen, R., Wang, L., An, Z., Chen, X. and Chen, P. (2021) Effect of *Π*- Conjugation Units on The Liquid Crystal and Photovoltaic Performance of Heterocyclic Pyridine-Based Compounds. *Liquid Crystals*, **48**, 2178–2187.

52. Emsley, J. W. (2025) The Structure and Orientational Order of Molecules in Nematic Liquid Crystal Phases. *Progress in Nuclear Magnetic Resonance Spectroscopy*, **101576**.

53. Oliveira, I. S., Loureiro, E. C., Garcia-Rio, L. and Marques, E. F. (2025) Tuning the Formation of Thermotropic Ionic Liquid Crystals Through the Spacer Length in 14-S-14 Gemini Surfactants. *Journal of Molecular Liquids*, **128334**.

54. Strachan, G. J., Harrison, W. T. A., Storey, J. M. D. and Imrie, C. T. (2025) Understanding the Remarkable Difference in Liquid Crystal Behaviour between Secondary and Tertiary Amides: The Synthesis and Characterisation of New Benzanilide-Based Liquid Crystal Dimers. *Physical Chemistry Chemical Physics*, **23**, 12600–12611.

55. Gonçalves, I. L., da Rosa, R. R., Eifler-Lima, V. L. and Merlo, A. A. (2020) The use of isoxazoline and isoxazole scaffolding in the design of novel thiourea and amide liquid-crystalline compounds. *Beilstein Journal of Organic Chemistry*, **16**, 175–184.

56. Al-Hamdani, U. J., Abbo, H. S., Shaheeb, E. H. and Titinchi, S. J. J. (2019) Symmetrical and Asymmetrical Liquid Crystal Dimers: Synthesis, Characterisation and Mesomorphic Behaviour. *Liquid Crystals*, **46**, 2291–2300.

57. Nada, S., Hagar, M., Farahat, O., Hasanein, A. A., Emwas, A. H., Sharfalddin, A. A., Jaremko, M. and Zakaria, M. A. (2022) Three Rings Schiff Base Ester Liquid Crystals: Experimental and Computational Approaches of Mesogenic Core Orientation Effect, Heterocycle Impact. *Molecules*, **27**, 2304.

58. Bernardino, K., Zhang, Y., Ribeiro, M. C. C. and Maginn, E. J. (2020) Effect of Alkyl-Group Flexibility on The Melting Point of Imidazolium-Based Ionic Liquids. *The Journal of Chemical Physics*, **153**, 044504.

59. Donaldson, T., Staesche, H., Lu, Z. B., Henderson, P. A., Achard, M. F. and Imrie, C. T. (2010) Symmetric and Non-Symmetric Chiral Liquid Crystal Dimers. *Liquid Crystals*, **37**, 1097–1110.

60. Rachwalski, M. (2023) Special Issue: Asymmetry and Symmetry in Organic Chemistry. *Symmetry*, **15**, 1363.

61. Mohammady, S. Z., Aldhayan, D. M., Alshammri, M. A., Alshammari, A. K., Alazmi, M., Katariya, K. D., Jaremko, M. and Hagar, M. (2021) Polar alkoxy group and pyridyl effects on the mesomorphic behavior of new non-symmetrical Schiff base liquid crystals. *Symmetry*, **13**, 1832.

62. Amiruddin, N. S., Jamain, Z. and Khairuddean, M. (2023) Synthesis, Characterization and Liquid Crystalline Behavior of 4-((E)-(((E)-4-(Decyloxy) Benzylidene) Hydrazineylidene)Methyl)Phenol. *Malaysian Journal of Chemistry*, **25**, 517–524.

63. Jamain, Z., Omar, N. F. and Khairuddean, M. (2020) Synthesis and Determination of Thermotropic Liquid Crystalline Behavior of Cinnamaldehyde-Based Molecules with Two Schiff Base Linking Units. *Molecules*, **25**, 3780.

64. Ahmed, H., Hagar, M. and Saad, G. (2019) Impact of The Proportionation of Dialkoxy Chain Length on The Mesophase Behavior of Schiff Base/Ester

Liquid Crystals; Experimental and Theoretical Study. *Liquid Crystals*, **46**, 1611–1620.

65. Jamain, Z., Khairuddean, M., Kamaruddin, K. and Rui, Y. Z. (2021) Synthesis, Structural Elucidation and Mesophase Behaviour of Hexasubstituted Cyclotriphosphazene Molecules with Amide Linking Unit. *Malaysian Journal of Chemistry*, **23**, 213–225.

66. Markiewicz, R., Klimaszyk, A., Jarek, M., Taube, M., Florczak, P., Kempka, M., Fojud, Z. and Jurga, S. (2021) Influence of Alkyl Chain Length on Thermal Properties, Structure, and Self-Diffusion Coefficients of Alkyltriethylammonium-Based Ionic Liquids. *International Journal of Molecular Sciences*, **22**, 5935.